Material effects on dynamics in triple-nozzle gas-puff Z pinches

J. Narkis ,* F. Conti , and F. N. Beg
Center for Energy Research, University of California San Diego, La Jolla, California 92093, USA

(Received 27 November 2021; accepted 15 March 2022; published 13 April 2022)

The gas-puff Z pinch has a long history with myriad applications as an efficient neutron or x-ray source. Its simplicity as a load configuration makes it suitable for studying fundamental plasma physics phenomena such as instabilities and energy transport. For example, the implosion of cylindrical shells onto a fusion fuel are inherently susceptible to instability growth on their external surfaces; if such instabilities are unmitigated, then the consequences in terms of degraded performance can be substantial. Similarly, mitigating heat transport from a hot fuel to its colder surrounding container can make fusion conditions more easily achievable. Here we have conducted a systematic study of triple-nozzle (outer liner, inner liner, fuel) gas puffs using two-dimensional (2D) magnetohydrodynamic simulations to investigate the effect of load material on the relevant dynamics. Analogous to past studies on spherical blast waves and converging shock waves, a trend emerges linking increased radiative cooling, lower adiabatic index, and increased magneto-Rayleigh-Taylor instability growth. Notably, our results suggest that, for the present configuration, Ar radiates less than both Ne and Kr during the early stages of the implosion while mass is being swept up and perturbations begin to seed instability growth. Consequently, pinches with Ar on the outer surface exhibit more stable 2D behavior. Here we also present a parameter scan of thermonuclear neutron yield, Y, as a function of peak current, I_{pk} and dopant concentration with Ne or Ar, depending on the inner liner material. Above 6 MA, our results suggest $Y \propto I_{\mathrm{pk}}^5$ and even substantial mixing (10% by volume) of Ne into the fuel does not drastically reduce yield, suggesting an Ar/Ne/fuel configuration may reliably achieve DD thermonuclear yields of 10^{13}–10^{14}/cm in the 10–20 MA range.

DOI: 10.1103/PhysRevE.105.045205

I. INTRODUCTION

The Z pinch is a conceptually simple plasma configuration with a long history of wide-ranging applications [1,2] in which an applied axial current interacts with the self-generated azimuthal magnetic field to radially compress the load. Examples include deuterium-fiber Z pinches [3–5], which were among the first concepts explored for fusion, but were ultimately unsuccessful due to the unavoidable onset of plasma instabilities; wire-array Z-pinches [6], which can be used to generate immense x-ray power and energy, as evidenced by experiments at Sandia National Laboratories which produced ∼200 TW and ∼2 MJ of x-rays with tungsten wire arrays at the Z pulsed power facility [7]; and gas-puff Z pinches [8], which have predominantly been explored as an efficient K-shell x-ray source [9–12], but have also received some attention as a neutron source, either as pure deuterium [13,14] or a hybrid configuration [15,16] in which using a high-atomic-number outer shell (or "liner") increases load compressibility, and thus yield, due to enhanced radiative cooling. Here, we focus on this lattermost configuration.

As with other inertial confinement fusion (ICF) schemes like laser-driven ICF [17] and pulsed-power-driven magnetized liner inertial fusion (MagLIF) [18], compressing the fuel in a hybrid gas-puff to the temperatures and densities to produce substantial yield requires mitigating instability growth. Though the seeding mechanisms vary, an instability common to all these schemes is the Rayleigh-Taylor instability [19–21], which develops at the interface between a heavier fluid and a lighter fluid, with the lighter fluid driving the acceleration. In pulsed-power-driven implosions such as MagLIF and gas-puff Z pinches, the lighter fluid is the vacuum magnetic field and the instability is aptly called the magneto-Rayleigh-Taylor instability (MRTI) [22]. There are numerous approaches to MRTI mitigation [8]; among these approaches are density-profile tailoring [23,24], whereby the implosion trajectory is altered by adjusting the initial density profile of the load, and axial premagnetization, whereby an axial magnetic field embedded within the load and amplified during the implosion due to flux compression smooths out perturbations via field-line tension [16,25]. Previous work demonstrated with radiation magnetohydrodynamic (MHD) simulations that combining these two mitigation strategies could be advantageous [26]. It was shown that adding a second Ne "liner" to a neon-on-deuterium multishell pinch lowered the required axial field, B_{z0}, to stabilize the pinch by roughly half. Consequently, the pinch was stabilized without significant penalty in thermonuclear neutron yield. However, the degree to which the liner material affects MRTI growth, as well as other dynamics that could affect neutron yield, remains an open question. Various effects, including resistivity, radiative cooling, and pinch compressibility are inextricably coupled and dependent on liner material. Here we investigate the interaction of these effects

*narkis1@llnl.gov; Lawrence Livermore National Laboratory, Livermore, California 94550, USA.

with a systematic study using one-dimensional (1D) and 2D radiation MHD simulations.

For any neutron-producing configuration driven by pulsed power, it is natural to question how the neutron yield scales to larger devices. The conventional understanding is that neutron yield for pure deuterium loads will scale approximately as peak current, I_{pk}, to the fourth power [27]. This scaling occurs regardless of whether the origin of the yield is beam-target or thermonuclear [28]. The second objective of this work is to investigate whether similar scaling is observed with multi-material pinches. In addition to scaling I_{pk}, we also consider the effect of liner mixing into the fuel. For ICF concepts that are pursuing ignition, it is well known that fuel mixing can drastically reduce neutron yield because the higher-Z contaminants are much more radiative, cooling the fuel as a result [29,30]. On the other hand, it has been observed in dense plasma focus experiments at currents up to 2 MA that a small amount of high-Z dopant can increase yield [31]. Here we present simulation results elucidating the potential transition from dopants having a beneficial effect to one that is more harmful.

The remainder of the manuscript is organized as follows: Section II describes the simulation setup, Sec. III presents results for $I_{\mathrm{pk}} = 850$ kA simulations, Sec. IV discusses results of simulations investigating neutron yield scaling with I_{pk} and dopant percentage, and Sec. V contains concluding remarks.

II. SIMULATION SETUP

The multiphysics radiation-MHD code HYDRA [32] is used for the simulations discussed here. HYDRA is an arbitrary Lagrangian Eulerian code with multiple radiation transport models; here the multigroup radiation diffusion with nonlocal thermodynamic equilibrium (non-LTE) opacities is used [33]. The resistive MHD equations are solved self-consistently with a coupled external circuit having the two-loop structure shown in Ref. [34], including the reported increase to inductance to improve agreement with experimental data. Ions and electrons have separate temperatures. Epperlein-Haines Lee-More transport coefficients are used with modified thermal conductivities such that the parallel and perpendicular coefficients are equal with zero Hall parameter. Ions are treated as an ideal gas, and the electron EOS is calculated via the opacity package. Postprocessing is completed with the open-source code YORICK and Mathworks MATLAB.

The triple-nozzle gas-puff load is initialized in the simulation domain with a uniform temperature of 1 eV, anode-cathode length of 1 cm, and the initial mass density profile (normalized to $I_{\mathrm{pk}}^2[\mathrm{MA}^2]$) shown in Fig. 1. Normalization in this manner imposes comparable zero-dimensional (0D) dynamics at an arbitrary peak current, a requisite for scaling studies. This is demonstrated, for example, by invoking the thin-shell model to obtain a dimensionless scaling parameter, Π,

$$\Pi \propto \frac{I_{\mathrm{pk}}^2 \tau^2}{\hat{m} R_0^2} \propto \frac{I_{\mathrm{pk}}^2 \tau^2}{\rho_0 R_0^4}, \tag{1}$$

where τ is the implosion timescale, $\hat{m} = \rho_0 R_0^2$ is the mass per unit length, ρ_0 is initial density, and R_0 is initial radius [1].

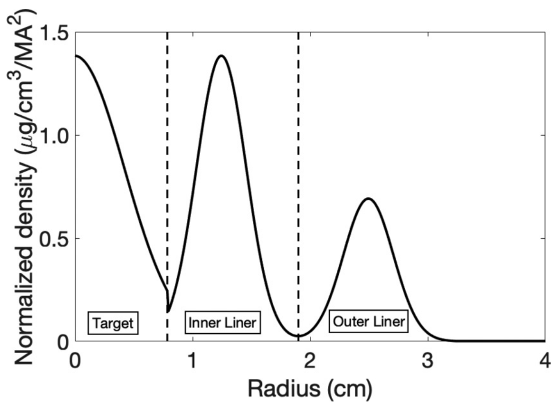

FIG. 1. Initial radial density profile used in the simulations, normalized to peak current squared. Dashed lines indicate material interfaces.

The load is coupled to the CESZAR linear transformer driver [34], and the charging voltage is scaled linearly to provide the desired peak current, e.g., 200 kV gives an approximate peak current of 850 kA, and 2.35 MV gives 10 MA. The current rise time is ~140–150 ns for this load geometry; see Ref. [26] for current traces at 200 kV. We note that scaling density and current in this manner may not be experimentally practical, but redesigning a load and driver at each current level is beyond the scope of this work and would introduce an additional level of complexity that would make the phenomena studied here, e.g., magneto-Rayleigh-Taylor instability growth, more challenging to study systematically.

The pre-embedded axial magnetic field is scaled linearly, with a base value of $B_{z0} = 0.3$ T at 850 kA. The approach to scale axial magnetic field linearly with peak current is supported by a stability analysis of a dynamic Z pinch with an embedded axial magnetic field [35]. In this work, the authors showed that the axial magnetic field required to stabilize the pinch is a relatively small fraction of the azimuthal magnetic field, which scales as the ratio of current to pinch radius. It was shown that the required initial field to stabilize the pinch, B_{st}, can be approximately given by

$$B_{\mathrm{st}}\,[\mathrm{T}] = \frac{I_{\mathrm{pk}}\,[\mathrm{MA}]}{R_0\,[\mathrm{cm}]}. \tag{2}$$

The simulation is divided into three regions, indicated by dashed lines in Fig. 1: the deuterium fuel or "target" in the center; the "inner liner" of Ne, Ar, or Kr initially between ~0.8 and ~1.9 cm; and the "outer liner" of Ne, Ar, or Kr from ~1.9 to ~3.1 cm. Peak mass density for the 850-kA simulations were 1.0, 1.0, and 0.5 μg/cm^3 for the target, inner liner, and outer liner, respectively. Full width at half maxima (FWHM) were 1 cm and 0.5 cm for the target and liners, respectively. Axial uniformity and a $\pm 1\%$ density perturbation are initialized in 2D simulations to seed instability growth.

III. DYNAMICS AT $I_{\mathrm{pk}} = 850$ kA

The 0D dynamics, i.e., implosion trajectory and pinch time, are a function of load mass distribution and peak current, both of which are mostly independent of liner material. A typical implosion proceeds as follows: For the first ~100 ns, the magnetic piston sweeps up the outer liner and after it is swept up, the B_z tension is insufficient to mitigate MRTI growth; between ∼100 and ∼140 ns, the outer liner merges with the inner liner and instability amplitudes decrease or remain constant; after ∼140 ns, the liners have merged and MRTI growth resumes and then the pinch stagnates on axis at ∼160 ns. This is summarized in Fig. 2(a), which shows mass density contours for the Ar outer liner, Ne inner liner configuration in 15 ns increments leading up to bang time, the time at which dN/dt is at a maximum, where N is the number of thermonuclear neutrons produced from the DD reaction; a similar set of images with a Ne outer liner is shown in Fig. 5(b) of Ref. [26].

Instability growth as a function of wavelength is quantified here by performing a fast Fourier transform (FFT) on the radially integrated mass as a function of axial position. Amplitudes are normalized to the total mass per unit length, which allows for straightforward comparison across a range of values for I_{pk}. An example of this is shown in Fig. 2(b), which shows normalized instability amplitude as a function of wavelength and time for the Ar-outer-liner, Ne-inner-liner simulation with $I_{\mathrm{pk}} = 850$ kA for the 100-ns period preceding the bang time of 159.4 ns. From these data, we see that for this particular simulation, the $\lambda = 2$ mm mode is dominant both before and after the liners merge, with amplitudes shown in Fig. 2(c). On merging of the liners, MRTI growth is effectively delayed by ∼25 ns: The maximum instability amplitude prior to the liners merging of $\sim 5.0 \times 10^{-4}$ is first reached at 121 ns, and this value is not surpassed until 146 ns. A maximum amplitude of 1.5×10^{-3} is observed at 156 ns.

In order to compare instability amplitude between configurations, it is useful to consider a mode-independent metric like Fourier spectral power, $\mathscr{P}$, defined here as

$$\mathscr{P}(t) \equiv \int |\hat{f}(k,t)^2| dk, \tag{3}$$

where $\hat{f}$ is normalized FFT amplitude. As shown in Fig. 3, instability growth is reduced in the Ar-outer-liner, Ne-inner-liner simulation relative to the Ne-outer-liner, Ne-inner-liner simulation. This can also be seen in the dominant mode growth, which is $\lambda = 2$ mm for both simulations; see Fig. 6 of Ref. [26]. The trend of increasing stability does not continue for the Kr-outer-liner, Ne-inner-liner configuration. There is significant long-mode structure observed in this simulation that is not reduced when the liners merge; the dominant mode is $\lambda = 5$ mm. This is because longer-wavelength growth is more challenging to mitigate with an axial magnetic field, because the stabilizing term is proportional to the instability wave number, k. There are additional modes at ∼1 mm with significant amplitudes at peak compression. Combined, these results explain the greater spectral power for the Kr-outer-liner configuration.

The increased stability in the Ar outer liner relative to either the Ne outer liner or Kr outer liner is notable because physical explanations for varying stability among species tend to be attributed to phenomena that would be expected to produce trends that are monotonic with atomic number. For example, it has been hypothesized [8] that instability amplitude can be reduced via resistive diffusion, hence one might

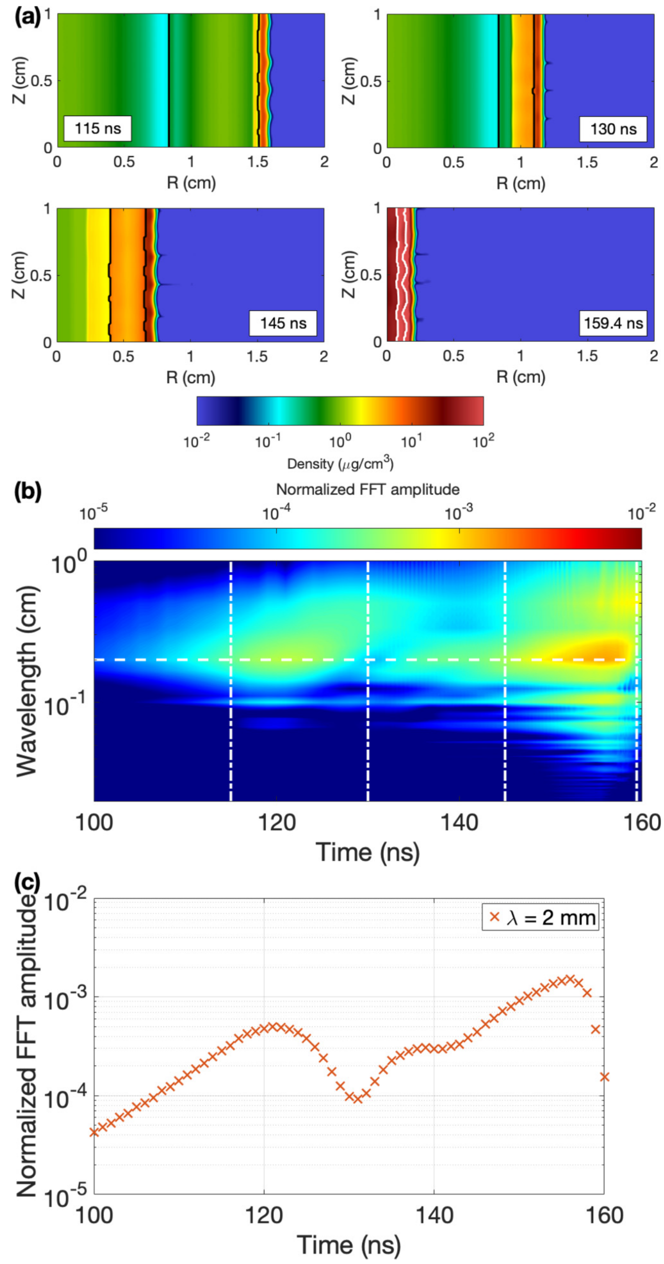

FIG. 2. (a) Mass density contours for the Ar-outer-liner, Ne-inner-liner simulation with $I_{\mathrm{pk}} = 850$ kA. Contours are shown in 15-ns intervals leading up to bang time. The interfaces between inner liner and outer liner and inner liner and target are denoted by solid black or white lines. (b) Fast Fourier transform (FFT) amplitude of radially-integrated density in the 60 ns prior to bang time for the same load configuration. Amplitude is normalized to the mass per unit length of the load. The vertical white dashed lines correspond to the mass density contours shown in (a). The horizontal white dashed line is the amplitude of the dominant mode, $\lambda = 2$ mm, corresponding to the plot shown in (c).

expect increasing stability from Ne to Ar to Kr, since resistivity tends to increase with atomic number.

One possible explanation draws an analogy to work on spherical blast waves, either propagating through an ambient medium [36–39] or in a convergent geometry [40,41]. These works, taken in aggregate, establish a correlation between

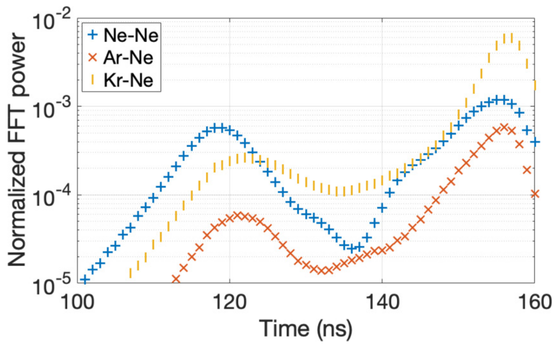

FIG. 3. FFT spectral power of radially integrated density in the 60 ns prior to bang time for the three Ne-inner-liner configurations calculated according to Eq. (3).

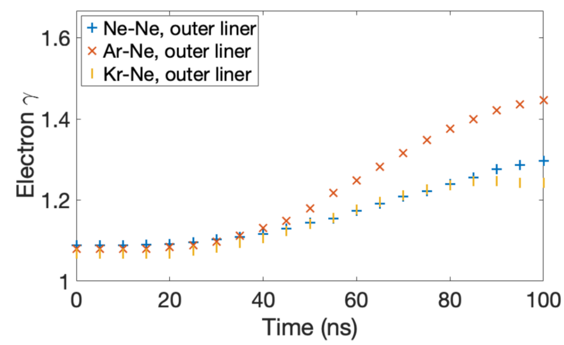

FIG. 4. Mass-averaged adiabatic index of the electrons in the outer liner for the three Ne-inner-liner configurations, calculated according to Eq. (4).

enhanced stability and higher adiabatic index, γ. It was observed in Ref. [37] that the shock propagating through N was stable, but the shock propagating through Xe was highly unstable. A γ of 1.3 ± 0.1 was calculated for N, whereas $\gamma = 1.06 \pm 0.02$ was inferred for Xe. The authors attribute this to greater radiation by Xe, which will increase the degrees of freedom within the gas, lowering γ. Noting from theoretical estimates [36] that such blast waves will become unstable for $\gamma < 1.2$, they conclude that greater radiation by Xe is the driver behind the observed instability. Later work [39] also found that the shock speed must be of sufficient strength to drive significant radiative cooling; otherwise, the instability may not develop [38]. In convergent geometry, Ref. [40] showed using the Chester-Chisnell-Whitam approximation that all modes of a spherically converging shock in a $\gamma = 7/5$ gas were unstable, and the more recent, rigorous work in Ref. [41] showed that above a certain mode number, perturbations are smeared out, but the range and growth rate of unstable modes is larger for $\gamma = 7/5$ than for $\gamma = 5/3$. There has also been theoretical work studying the effect of γ on Rayleigh-Taylor instability growth at an interface between two fluids. Consistent with the aforementioned studies on blast waves, Refs. [42] and [43] both predict that stability increases with γ, though Ref. [43] notes that increased stability with higher γ may be offset with reduced stability with increasing sound speed.

It is therefore potentially insightful to consider the effective adiabatic indices of the loads used here. In these simulations, the ions are treated as a monatomic ideal gas. The electron equation of state is calculated self-consistently with the radiation transport model, and the adiabatic constant for electrons, γ_e, varies both spatially and temporally. The effective value for γ_e for each cell can be extracted via outputted values of the electron temperature (T_e), density (ρ), electron pressure (p_e), and electron specific heat capacity ($c_{\rm pe}$) by adopting Eqs. (11)–(13) from Ref. [44]. Taking molecular weight to be constant, we can write

$$\gamma_e = 1 + \frac{p_e}{\rho c_{\rm ve} T_e}; \tag{4}$$

a similar calculation for ions gives the expected unvarying value of $\gamma_i = 5/3$. The mass-averaged value of γ_e at early times is significantly higher for the Ar-outer-liner, Ne-inner-liner configuration than for either the Kr-outer-liner or Ne-outer-line configuration, as shown in Fig. 4. Noting that the second term of Eq. (4) is proportional to $Z/m_i c_{\rm pe}$, where Z is average ionization state and m_i is ion mass, we can attribute the lower γ_e for Ne to a larger specific heat capacity. The lower γ_e for Kr is attributable to the ratio of Z/m_i; in the 10s of eV range, which is characteristic of T_e in the early stages of the implosion, $Z_{\rm Kr}/Z_{\rm Ar}$ is close to unity, but Kr is twice as heavy. For example, at 100 ns the Ne outer liner has $Z = 7.1$, $c_{\rm pe} = 129$ MJ/g/KeV; the Ar outer liner has $Z = 8.1$, $c_{\rm pe} = 46$ MJ/g/KeV; and the Kr outer liner has $Z = 10.4$, $c_{\rm pe} = 51$ MJ/g/KeV.

It is also interesting to note that early in the implosion, the Ar outer liner does appear to be radiating less than both the Ne and Kr pinches. Taking the same example at 100 ns, the Ne outer liner has $T_e = 45.6$ eV and ion density, $n_i = 9.8 \times 10^{16}$ cm^{-3}; the Ar outer liner has $T_e = 60.1$ eV, $n_i = 5.1 \times 10^{16}$cm^{-3}; and the Kr outer liner has $T_e = 52.9$ eV, $n_i = 2.4 \times 10^{16}$ cm^{-3}. Using the FLYCHK [45] code, estimated radiative powers for Ne, Ar, and Kr liners are 2.1×10^8, 1.3×10^8, and 2.3×10^8 W/cm^3, respectively. In physical terms, this would suggest that the increased stability of the Ar outer liner is related to its reduced radiative output at the temperatures and densities reached by the outer liner early in the implosion. As with previous studies in spherical geometry, there is evidence to suggest a correlation between greater radiative cooling, decreased adiabatic constant, and greater instability. However, in contrast to these previous studies, the data suggest increased radiative output may not strictly be monotonic with atomic number.

There is a more straightforward trend with regard to stability as a function of inner liner material. The increased compressibility is immediately apparent from density contours at similar times, shown in Figs. 5(a)–5(c). While the interface between the liner and target does appear more stable as inner liner Z is increased, the spectral FFT power is greater, as shown in Fig. 5(d). This greater instability on the plasma surface could be exacerbated by 3D effects, which could increase the likelihood of instability feedthrough to the fuel region.

Neutron yield and associated quantities as a function of inner liner material and outer liner material are summarized in Table I. Broadly speaking, one would expect, all other dynamics similar, that a higher-Z inner liner and/or outer liner will be more radiative and compressible, which would result

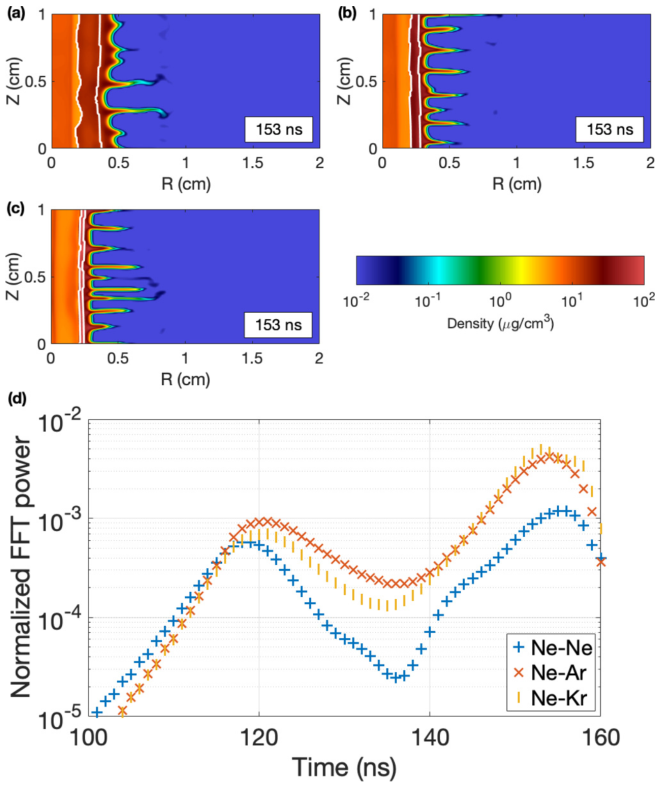

FIG. 5. Density contours at $t = 153$ ns for (a) the Ne-outer-liner, Ne-inner-liner configuration; (b) the Ne-outer-liner, Ar-inner-liner configuration; and (c) the Ne-outer-liner, Kr-inner-liner configuration. Material interfaces are indicated by the white solid lines. (d) Normalized FFT spectral power of radially integrated density in the 60 ns prior to bang time for the three Ne-inner-liner configurations, calculated according to Eq. (3).

in greater fuel compression, and thus higher peak temperature, peak density, and neutron yield. There is clearly increased compression for higher-Z inner liners, as shown both by Fig. 5(a)–5(c) and Table I. The correlation to increased compression is reduced for higher-Z outer liners but still present.

If losses are comparable between two configurations and the extra compression is approximately adiabatic, then peak temperature will increase as convergence ratio (C_R), the ratio of initial to final radius, to the $4/3$ power for cylindrical geometry. The Ne-inner-liner and Ar-inner-liner configurations are on similar adiabats, but the Kr-inner-liner clearly lowers the ion fuel adiabat and thus yield. There are two possible explanations, but only one is plausible. First, the electrons within the Kr inner liner could be colder, and so the fuel electrons lose energy via thermal conduction, then causing the fuel ions to lose energy via electron-ion equilibration. This is implausible for two reasons: (1) with $B_{z0} = 0.3$ T, the electron Hall parameter greatly exceeds unity (e.g., Ref. [26] calculates the average fuel electron Hall parameter at bang time to be 723), so electron thermal conduction is magnetically inhibited, (2) the electron-ion equilibration timescale would have to be comparable to the dwell time; it is much larger at 850 kA such that T_i and T_e are essentially decoupled—we tangentially note T_e is lower than T_i due to bremsstrahlung. The only other possibility is that there are significant ion thermal conduction losses from the fuel to the inner liner. One can therefore conclude that, in combination with the effectiveness of snowplow stabilization, a lower-Z inner liner is more likely to be the optimal choice.

TABLE I. One-dimensional neutron yield (Y_{DD}), target convergence ratio (ratio of initial radius, r_0, to final radius, r_f), mass-averaged peak target ion temperature ($T_{i,\mathrm{pk}}$), and mass-averaged peak target electron temperature ($T_{e,\mathrm{pk}}$) for the tested load configurations.

Load	Y_{DD} (x10^9)	r_0/r_f	$T_{i,\mathrm{pk}}$ (keV)	$T_{e,\mathrm{pk}}$ (keV)
Ne-Ne-D	1.3	9.7	7.6	1.8
Ne-Ar-D	2.9	10.8	9.0	2.0
Ne-Kr-D	2.4	12.1	8.0	2.3
Ar-Ne-D	1.7	10.1	8.1	2.0
Ar-Ar-D	4.0	11.3	9.7	2.1
Ar-Kr-D	3.5	13.8	9.3	2.7
Kr-Ne-D	1.9	10.1	8.0	1.9
Kr-Ar-D	4.2	11.5	9.7	2.1
Kr-Kr-D	3.6	13.7	8.9	2.6

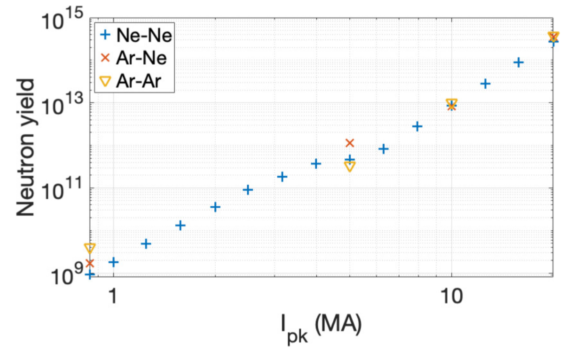

FIG. 6. Neutron yield as a function of peak current, I_{pk} for the Ne-outer-liner, Ne-inner-liner, Ar-outer-liner, Ne-inner-liner, and Ar-outer-liner, Ar-inner-liner configurations. At lower currents, yield scales as $I_{\mathrm{pk}}^{4.2}$. Above 6 MA, yield scales as $I_{\mathrm{pk}}^{5.0}$. Between Ne and Ar, yield is not significantly affected by liner material, particularly at higher currents.

IV. NEUTRON YIELD SCALING WITH VARYING I_{pk} AND DOPANT PERCENTAGE

Neutron yield scalability with current was investigated for three configurations: Ne-outer-liner, Ne-inner-liner; Ar-outer-liner, Ne-inner-liner; and Ar-outer-liner, Ne-inner-liner. One-dimensional simulations were performed due to limited computing resources. Figure 6 shows the neutron yield scaling as a function of peak current. As stated previously, neutron yield for pure deuterium pinches scales as I_{pk}^4. Up to 2 MA, we observe this scaling. Between ~2 and ~5 MA, yield scales less: this is attributable to increased bremsstrahlung from fuel electrons that scales with density, and consequently peak T_i and burn width are reduced. However, beyond ~6 MA, peak T_i, peak T_e, and burn width all increase with current. This can be attributed to the increasing optical thickness of the liners; fuel energy loss due to bremsstrahlung becomes increasingly more difficult to absorb or transmit, and is thus reabsorbed

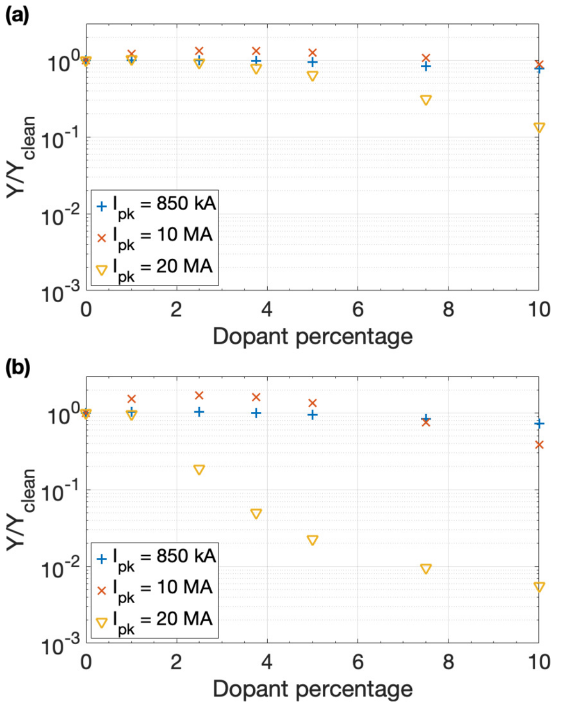

FIG. 7. Neutron yield relative to the "clean," i.e., zero dopant, simulation at $I_{\rm pk} = 850$ kA, 10 MA, and 20 MA for the (a) Ar-outer-liner, Ne-inner-liner, Ne-doped fuel and the (b) Ar-outer-liner, Ar-inner-liner, Ar-doped fuel as a function of dopant percentage, up to 10% by volume.

by the fuel. Additionally, the radiation that is absorbed will rapidly heat the electrons at the fuel/liner interface, potentially providing additional mitigation of fuel electron thermal conduction losses.

Though at higher currents there is little to distinguish between Ar and Ne as liner materials, in an experiment it would be expected that a degree of inner liner material may mix into the target. To study the effect of mixing in the fuel at various current levels, here we impose up to a 10% (by volume) dopant of inner liner material. The dopant is added at $t = 0$ and remains at a constant fraction throughout the fuel. The results are shown for Ar-outer-liner, Ne-inner-liner in Fig. 7(a) and for Ar-outer-liner, Ar-inner-liner in Fig. 7(b), where yield has been normalized to the "clean" (0% dopant) simulation at each current level. For both materials, yield reduction at 850 kA is insignificant, 20–30% with 10% dopant. At 10 MA, dopant is seen to increase yield at a few percentages, then becomes deleterious as the percentage continues to increase; this trend is more prominent with Ar, which gave $Y/Y_{\rm clean} = 170\%$ at 2.5% Ar, dropping to $Y/Y_{\rm clean} = 40\%$ at 10% Ar. At 20 MA, no amount of dopant is beneficial. These results suggest an implosion on a hypothetical ∼10 MA driver using a Ar-outer-liner, Ne-inner-liner, or Ar-outer-liner, Ar-inner-liner configuration could produce yields comparable to those predicted by clean simulations even with significant mixing.

However, it was found that scaling B_z linearly with $I_{\rm pk}$ does not result in comparable instability amplitudes. Simulations performed at $I_{\rm pk} = 850$ kA, 5 MA, and 10 MA, for all three Ne-inner-liner simulations, showed increasing amplitudes from 850 kA to 5 MA and again from 5 to 10 MA.

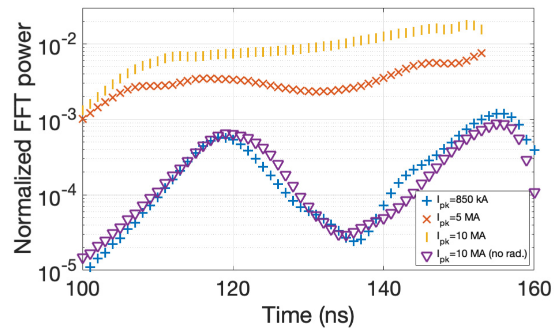

FIG. 8. FFT spectral power of radially-integrated density in the 60 ns prior to bang time for four Ne-outer-liner, Ne-inner-liner configurations: $I_{\rm pk} = 850$ kA, $I_{\rm pk} = 5$ MA, $I_{\rm pk} = 10$ MA, and $I_{\rm pk} = 10$ MA with radiation suppressed. Note that bang time for $I_{\rm pk} = 5$ MA and $I_{\rm pk} = 10$ MA with radiation is ∼153 ns.

This can, in fact, be attributed to enhanced radiative cooling due to the increased load density; the 5- and 10-MA simulations are 35× and 138× heavier than the 850-kA simulations, respectively.

To confirm the predominant driver of instability growth here is radiative losses, a simulation with radiation disabled for the Ne-outer-liner, Ne-inner-liner configuration for $I_{\rm pk} = 10$ MA was conducted. Instability amplitudes were reduced to those seen in the $I_{\rm pk} = 850$ kA simulation. For example, Fig. 8 shows the FFT spectral power for Ne-outer-liner, Ne-inner-liner simulations for $I_{\rm pk} = 850$ kA, 5 MA, 10 MA, and 10 MA with no radiation. Furthermore, while it was observed that the outer-liner γ_e is lower for both $I_{\rm pk} = 10$ MA simulations relative to the $I_{\rm pk} = 850$ kA simulation, the decrease is greater when radiation is enabled. For example, at $t = 100$ ns, $\gamma_e = 1.30, 1.23,$ and 1.14 in the outer liner for $I_{\rm pk} = 850$ kA, $I_{\rm pk} = 10$ MA without radiation, and $I_{\rm pk} = 10$ MA with radiation, respectively.

V. CONCLUSION

The primary result of this work is a possible explanation as to why Ne, Ar, and Kr gas puff Z pinches exhibit differences in instability growth despite being identically massed and having nearly identical implosion trajectories in resistive MHD simulations. Previous work on blast waves propagating through a high-atomic-number gas, Xe, was unstable relative to the same waves propagating through a lower-atomic-number gas, N [37], which was attributed to a lower effective adiabatic index due to enhanced radiative cooling. We observe a similar trend here, in that the Ar-outer-liner is more stable at early times and a higher effective electron adiabatic index, γ_e, than either Ne-outer-liner or Kr-outer-liner implosions. Relative to Ar, the Ne-outer-liner has a greater specific heat capacity, $c_{\rm pe}$, and the Kr-outer-liner is more difficult to ionize, i,e., Z/m_i is lower for Kr than for Ar. Both of these effects could be related to greater radiative cooling losses in Kr and Ne than Ar in the outer liner.

We also found that using a higher-atomic-number inner liner and/or outer liner increased fuel compression and thermonuclear neutron yield, except when the inner liner is changed from Ar to Kr. When a Kr inner liner is used, there is evidence to suggest significant ion thermal conduction losses from the hot fuel to the colder inner liner.

There were several notable results pertaining to the presented configuration scaling with peak current. First, neutron yield as a function of peak current, I_{pk} for a hybrid pinch like those presented here appear to scale greater than pure deuterium pinches; $Y \propto I_{pk}^5$ above 6 MA vs. I_{pk}^4, respectively. Second, there is evidence to suggest mixing of Ne or Ar of 10% by volume into the fuel is not deleterious for $I_{pk} = 850$ kA or 10 MA, but it is for $I_{pk} = 20$ MA. Finally, instability growth is more difficult to suppress as I_{pk} is increased. Our results suggest this is unavoidable due to enhanced radiation as load mass is increased, so scaling B_z more than linearly with I_{pk} may be necessary.

All of the presented results would benefit greatly from companion experiments on various drivers, including university-scale drivers like CESZAR and other, higher-current drivers. We hope to conduct upcoming campaigns in order to investigate the observed phenomena experimentally.

ACKNOWLEDGMENTS

This material is based on work supported by the Department of Energy, National Nuclear Security Administration under Award No. DE-NA0003842. F.C. acknowledges support from the Department of Energy, National Nuclear Security Administration under Award No. DENA0004031. The authors thank A. Velikovich for useful discussions on gas-puff Z pinches and MRTI, and M. Marinak and Lawrence Livermore National Laboratory for access to and guidance in using the HYDRA code.

[1] D. D. Ryutov, M. S. Derzon, and M. K. Matzen, The physics of fast Z pinches, Rev. Mod. Phys. **72**, 167 (2000).

[2] M. G. Haines, A review of the dense Z-pinch, Plasma Phys. Control. Fus. **53**, 093001 (2011).

[3] O. A. Anderson, W. R. Baker, S. A. Colgate, J. Ise, and R. V. Pyle, Neutron production in linear deuterium pinches, Phys. Rev. **110**, 1375 (1958).

[4] J. D. Sethian, A. E. Robson, K. A. Gerber, and A. W. DeSilva, Enhanced Stability and Neutron Production in a Dense Z-Pinch Plasma Formed from a Frozen Deuterium Fiber, Phys. Rev. Lett. **59**, 892 (1987).

[5] I. R. Lindemuth, Two-Dimensional Fiber Ablation in the Solid-Deuterium Z Pinch, Phys. Rev. Lett. **65**, 179 (1990).

[6] S. V. Lebedev, R. Aliaga-Rossel, S. N. Bland, J. P. Chittenden, A. E. Dangor, M. G. Haines, and I. H. Mitchell, The dynamics of wire array Z-pinch implosions, Phys. Plasmas **6**, 2016 (1999).

[7] R. B. Spielman, C. Deeney, G. A. Chandler, M. R. Douglas, D. L. Fehl, M. K. Matzen, D. H. McDaniel, T. J. Nash, J. L. Porter, T. W. L. Sanford, J. F. Seamen, W. A. Stygar, K. W. Struve, S. P. Breeze, J. S. McGurn, J. A. Torres, D. M. Zagar, T. L. Gilliland, D. O. Jobe, J. L. McKenney *et al.*, Tungsten wire-array Z-pinch experiments at 200 TW and 2 MJ, Phys. Plasmas **5**, 2105 (1998).

[8] J. L. Giuliani and R. J. Commisso, A review of the gas-puff Z-pinch as an X-ray and neutron source, IEEE Trans. Plasma Sci. **43**, 2385 (2015).

[9] C. Deeney, P. D. LePell, B. H. Failor, J. S. Meachum, S. Wong, J. W. Thornhill, K. G. Whitney, and M. C. Coulter, Radius and current scaling of argon K shell radiation, J. Appl. Phys. **75**, 2781 (1994).

[10] B. Jones, J. P. Apruzese, A. J. Harvey-Thompson, D. J. Ampleford, C. A. Jennings, S. B. Hansen, N. W. Moore, D. C. Lamppa, D. Johnson, M. C. Jones, E. M. Waisman, C. A. Coverdale, M. E. Cuneo, G. A. Rochau, J. L. Giuliani, J. W. Thornhill, N. D. Ouart, Y. K. Chong, A. L. Velikovich, and A. Dasgupta, The effect of gradients at stagnation on K-shell x-ray line emission in high-current Ar gas-puff implosions, Phys. Plasmas **22**, 020706 (2015).

[11] A. J. Harvey-Thompson, C. A. Jennings, B. Jones, J. P. Apruzese, D. J. Ampleford, D. C. Lamppa, C. A. Coverdale, M. E. Cuneo, J. L. Giuliani, S. B. Hansen, M. C. Jones, N. W. Moore, G. A. Rochau, and J. W. Thornhill, Investigating the effect of adding an on-axis jet to Ar gas puff Z pinches on Z, Phys. Plasmas **23**, 101203 (2016).

[12] A. V. Shishlov, V. A. Kokshenev, N. E. Kurmaev, N. A. Labetskaya, F. I. Fursov, and R. K. Cherdizov, Generation of K-shell radiation of noble gases in the microsecond implosion regime, Rus. Phys. J. **62**, 1243 (2019).

[13] C. A. Coverdale, C. Deeney, A. L. Velikovich, J. Davis, R. W. Clark, Y. K. Chong, J. Chittenden, S. Chantrenne, C. L. Ruiz, G. W. Cooper, A. J. Nelson, J. Franklin, P. D. LePell, J. P. Apruzese, J. Levine, and J. Banister, Deuterium gas-puff Z-pinch implosions on the Z accelerator, Phys. Plasmas **14**, 056309 (2007).

[14] D. Klir, A. V. Shishlov, P. Kubes, K. Rezac, F. I. Fursov, V. A. Kokshenev, B. M. Kovalchuk, J. Kravarik, N. E. Kurmaev, A. Yu Labetsky, and N. A. Ratakhin, Deuterium gas puff Z-pinch at currents of 2 to 3 mega-ampere, Phys. Plasmas **19**, 032706 (2012).

[15] D. Klir, P. Kubes, K. Rezac, J. Cikhardt, J. Kravarik, O. Sila, A. V. Shishlov, B. M. Kovalchuk, N. A. Ratakhin, V. A. Kokshenev, A. Yu. Labetsky, R. K. Cherdizov, F. I. Fursov, N. E. Kurmaev, G. N. Dudkin, B. A. Nechaev, V. N. Padalko, H. Orcikova, and K. Turek, Efficient Neutron Production from a Novel Configuration of Deuterium Gas-Puff Z-Pinch, Phys. Rev. Lett. **112**, 095001 (2014).

[16] F. Conti, N. Aybar, J. Narkis, J. C. Valenzuela, H. U. Rahman, E. Ruskov, E. Dutra, S. Haque, A. Covington, and F. N. Beg, Study of stability in a liner-on-target gas puff Z-pinch as a function of pre-embedded axial magnetic field, Phys. Plasmas **27**, 012702 (2020).

[17] R. Betti and O. A. Hurricane, Inertial-confinement fusion with lasers, Nat. Phys. **12**, 435 (2016).

[18] S. A. Slutz, M. C. Herrmann, R. A. Vesey, A. B. Sefkow, D. B. Sinars, D. C. Rovang, K. J. Peterson, and M. E. Cuneo, Pulsed-power-driven cylindrical liner implosions of laser preheated

fuel magnetized with an axial field, Phys. Plasmas **17**, 056303 (2010).
[19] Lord Rayleigh, The form of standing waves on the surface of running water, Proc. Lond. Math. Soc. **s1-15**, 69 (1883).
[20] Geoffrey Ingram Taylor, The instability of liquid surfaces when accelerated in a direction perpendicular to their planes. I, Proc. R. Soc. Lond. A **201**, 192 (1950).
[21] Ye Zhou, Rayleigh-Taylor and Richtmyer-Meshkov instability induced flow, turbulence, and mixing. II, Phys. Rep. **723**, 1 (2017).
[22] E. G. Harris, Rayleigh-Taylor instabilities of a collapsing cylindrical shell in a magnetic field, Phys. Fluids **5**, 1057 (1962).
[23] Alexander L. Velikovich, F. L. Cochran, and J. Davis, Suppression of Rayleigh-Taylor Instability in Z-Pinch Loads with Tailored Density Profiles, Phys. Rev. Lett. **77**, 853 (1996).
[24] C. A. Jennings, D. J. Ampleford, D. C. Lamppa, S. B. Hansen, B. Jones, A. J. Harvey-Thompson, M. Jobe, T. Strizic, J. Reneker, G. A. Rochau, and M. E. Cuneo, Computational modeling of Krypton gas puffs with tailored mass density profiles on Z, Phys. Plasmas **22**, 056316 (2015).
[25] E. S. Lavine, S. V. Rocco, J. T. Banasek, W. M. Potter, J. B. Greenly, H. Wilhelm, N. Qi, D. A. Hammer, and B. R. Kusse, Implosion dynamics of triple-nozzle gas-puff z pinches on COBRA, Phys. Plasmas **28**, 022703 (2021).
[26] J. Narkis, F. Conti, A. L. Velikovich, and F. N. Beg, Mitigation of magneto-Rayleigh-Taylor instability growth in a triple-nozzle, neutron-producing gas-puff *Z* pinch, Phys. Rev. E **104**, L023201 (2021).
[27] B. L. Bures and Mahadevan Krishnan, An alternative scaling model for neutron production in Z-pinch devices, Phys. Plasmas **19**, 112702 (2012).
[28] A. L. Velikovich, R. W. Clark, J. Davis, Y. K. Chong, C. Deeney, C. A. Coverdale, C. L. Ruiz, G. W. Cooper, A. J. Nelson, J. Franklin, and L. I. Rudakov, Z-pinch plasma neutron sources, Phys. Plasmas **14**, 022701 (2007).
[29] A. J. Harvey-Thompson, M. R. Weis, E. C. Harding, M. Geissel, D. J. Ampleford, G. A. Chandler, J. R. Fein, M. E. Glinsky, M. R. Gomez, K. D. Hahn, S. B. Hansen, C. A. Jennings, P. F. Knapp, R. R. Paguio, L. Perea, K. J. Peterson, J. L. Porter, P. K. Rambo, G. K. Robertson, and G. A. Rochau, Diagnosing and mitigating laser preheat induced mix in MagLIF, Phys. Plasmas **25**, 112705 (2018).
[30] C. R. Weber, D. S. Clark, A. Pak, N. Alfonso, B. Bachmann, L. F. Berzak Hopkins, T. Bunn, J. Crippen, L. Divol, T. Dittrich, A. L. Kritcher, O. L. Landen, S. Le Pape, A. G. MacPhee, E. Marley, L. P. Masse, J. L. Milovich, A. Nikroo, P. K. Patel, and L. A. Pickworth, Mixing in ICF implosions on the National Ignition Facility caused by the fill-tube, Phys. Plasmas **27**, 032703 (2020).
[31] E. N. Hahn, D. Housley, J. Narkis, F. Conti, D. R. Lowe, and F. N. Beg, Effect of krypton admixture in deuterium on neutron yield in a megaampere dense plasma focus, J. Appl. Phys. **128**, 143302 (2020).
[32] M. M. Marinak, G. D. Kerbel, N. A. Gentile, O. Jones, D. Munro, S. Pollaine, T. R. Dittrich, and S. W. Haan, Three-dimensional HYDRA simulations of National Ignition Facility targets, Phys. Plasmas **8**, 2275 (2001).
[33] M. V. Patel, H. A. Scott, and M. M. Marinak, Enhanced NLTE atomic kinetics modeling capabilities in HYDRA, in *56th Annual Meeting of the APS Division of Plasma Physics*, APS Meeting Abstracts (APS, New Orleans, LA, 2014), Vol. 59, Abstract no. BAPS.2014.DPP.PO5.12.
[34] F. Conti, J. C. Valenzuela, V. Fadeev, N. Aybar, D. B. Reisman, A. Williams, G. Collins, J. Narkis, M. P. Ross, F. N. Beg, and R. B. Spielman, MA-class linear transformer driver for Z-pinch research, Phys. Rev. Accel. Beams **23**, 090401 (2020).
[35] A. B. Bud'ko, F. S. Felber, A. I. Kleev, M. A. Liberman, and A. L. Velikovich, Stability analysis of dynamic *Z* pinches and theta pinches, Phys. Fluids B: Plasma Phys. **1**, 598 (1989).
[36] E. T. Vishniac and D. Ryu, On the stability of decelerating shocks, Astrophys. J. **337**, 917 (1989).
[37] J. Grun, J. Stamper, C. Manka, J. Resnick, R. Burris, J. Crawford, and B. H. Ripin, Instability of Taylor-Sedov Blast Waves Propagating Through a Uniform Gas, Phys. Rev. Lett. **67**, 3200(E) (1991).
[38] M. J. Edwards, A. J. MacKinnon, J. Zweiback, K. Shigemori, D. Ryutov, A. M. Rubenchik, K. A. Keilty, E. Liang, B. A. Remington, and T. Ditmire, Investigation of Ultrafast Laser-Driven Radiative Blast Waves, Phys. Rev. Lett. **87**, 085004 (2001).
[39] J. M. Laming and J. Grun, Dynamical Overstability of Radiative Blast Waves: The Atomic Physics of Shock Stability, Phys. Rev. Lett. **89**, 125002 (2002).
[40] J. H. Gardner, D. L. Book, and I. B. Bernstein, Stability of imploding shocks in the CCW approximation, J. Fluid Mech. **114**, 41 (1982).
[41] M. Murakami, J. Sanz, and Y. Iwamoto, Stability of spherical converging shock wave, Phys. Plasmas **22**, 072703 (2015).
[42] I. B. Bernstein, Effect of compressibility on the Rayleigh-Taylor instability, Phys. Fluids **26**, 453 (1983).
[43] D. Livescu, Compressibility effects on the Rayleigh-Taylor instability growth between immiscible fluids, Phys. Fluids **16**, 118 (2004).
[44] M. A. de Avillez, G. J. Anela, and D. Breitschwerdt, Variability of the adiabatic parameter in monoatomic thermal and non-thermal plasmas, A&A **616**, A58 (2018).
[45] H.-K. Chung, M. H. Chen, W. L. Morgan, Y. Ralchenko, and R. W. Lee, FLYCHK: Generalized population kinetics and spectral model for rapid spectroscopic analysis for all elements, High Energy Dens. Phys. **1**, 3 (2005).